analytical chemistry

pubs.acs.org/ac Article

Direct Counting and Imaging Chain Lengths of Lipids by Stimulated Raman Scattering Microscopy

Zhiliang Huang,[#] Shuai Yan,[*,#] Yiran Li, Wei Ju, and Ping Wang

Cite This: *Anal. Chem.* 2023, 95, 5815−5819 Read Online

ACCESS | Metrics & More | Article Recommendations | Supporting Information

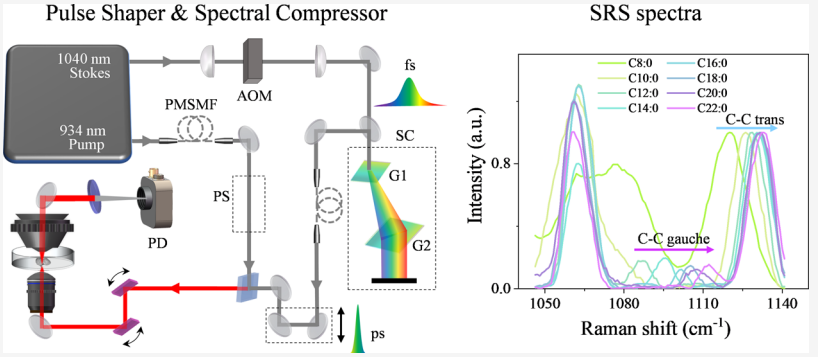

ABSTRACT: Direct counting and mapping the chain lengths of fatty acids on a microscopic scale are of particular importance but remain an unsolvable challenge. Although the current hyperspectral stimulated Raman scattering (SRS) microscopy has gained exceptional capability in chemical imaging of the degree of desaturation, the complete lipid characterization, including the carbon chain length quantification, is awaiting a major breakthrough. Here, we pushed the spectral resolution limit of hyperspectral SRS microscopy to 5.4 cm^{-1} by employing a highly efficient spectral compressor, which achieved spectral narrowing of the fs laser without much energy loss. The SRS imaging with such high spectral resolution enabled us to differ eight types of saturated lipids with carbon chain lengths from C8:0 to C22:0 by interrogating their subtly red-shifting Raman bands of alkyl C−C gauche stretches between 1070 and 1110 cm^{-1}. The SRS microscopy with superior spectral resolution will pave the way for comprehensive lipid characterization and contribute to uncovering the abnormal pathways of lipid metabolism in cancer.

The chemical alterations of fatty acids in diseased biological tissues are closely connected with aberrant functions of lipid metabolism at molecular and cellular levels.[1] Studies have shown that the degree of unsaturation, carbon chain length, and lipid metabolism in cancerous tissues significantly differ from that in normal tissues.[2,3] To identify the imperceptible lipid alternations in metabolic products of tissues, advanced chromatography, mass spectrometry, nuclear magnetic resonance (NMR), infrared, and Raman spectroscopy are routine analytical tools that are sensitive and accurate enough to decipher the lipid chain lengths, degree of desaturation, fat types, and their relative concentrations. However, all of these methods require elaborative lipid separation from their original specimens by various extracting solvents, hindering their in situ imaging applications. So far, very few imaging tools can provide the spatial distributions of lipid types by their chain lengths. Paul et al. generated a spectral training matrix capturing the variation caused in Raman-like spectra by unsaturated TAG (8:0, 16:1, 18:1, 18:2, 18:3, 20:4) at 1200−1786 and 2828−3102 cm^{-1}, and a least-squares decomposition was applied to map the average number of C═C double bonds and chain lengths in TAGs in native lipid droplets.[4] However, due to the limitation in spectral resolution of the employed broad-band coherent anti-Stokes Raman scattering (CARS) microscopy, it was still challenging to resolve the crowded and overlapped Raman bands in the C−H region. Over the past decade, advanced stimulated Raman scattering (SRS) microscopy has pushed the performance limits of Raman imaging in all aspects including sensitivity, speed, and spatial resolution and enabled delicate spatial and spectral characterization of biological tissues in various vital applications.[5−17] However, in all of these successes, the spectral resolution of SRS remained about 10 cm^{-1} or worse.[11,18] In particular, the subtle Raman shifts of C−C stretching, reflecting carbon chain lengths, vary only about 5 cm^{-1} in a 40 cm^{-1} spectral range between 1075 and 1115 cm^{-1} and are hardly resolved by the current SRS microscope.[19−23]

Received: January 18, 2023
Accepted: March 10, 2023
Published: March 21, 2023

https://doi.org/10.1021/acs.analchem.3c00291
Anal. Chem. 2023, 95, 5815−5819

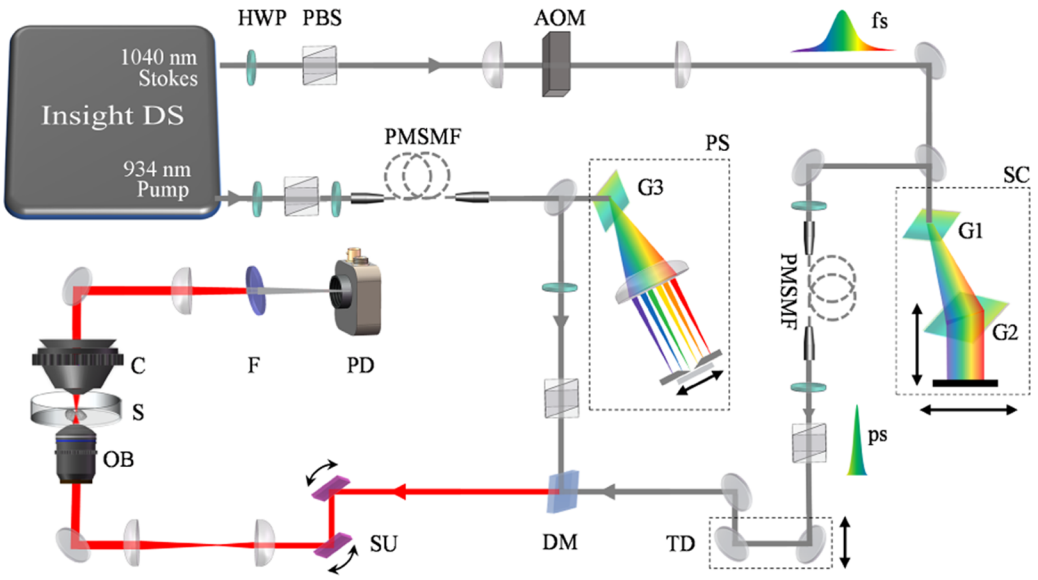

Figure 1. Schematic setup of the hyperspectral SRS microscope with superior spectral resolution. PBS: polarizing beam splitter, AOM: acousto-optic modulator, HWP: half-wave plate, PS: pulse shaper, SC: spectral compressor, PD: photodiode, DM: dichroic mirror, TD: time delay, PMSMF: polarization-maintaining single-mode fiber, SU: scanning unit, OB: objective, G: grating, C: condenser, S: sample, F: filter.

As a result, SRS microscopy with superior spectral resolution is highly desired for delicate chemical quantification and direct imaging of carbon chain lengths of lipids. Herein, for the first time, we pushed the limit of spectral resolution of SRS to ~5 cm^{-1} by an ultimate pulse shaper and spectral compressor and demonstrated quantitative chemical imaging of a phantom mixture of saturated lipids with varying carbon chain lengths from C8:0 (containing eight carbons in the fatty acid chain) to C22:0. The proof-of-concept experiment exploits the potential of complete spectral and spatial characterization of lipid chains in unprocessed tissues in situ.

EXPERIMENTAL SECTION

Hyperspectral SRS System with Ultimate Spectral Resolution. The dual-output femtosecond laser (InSight DeepSee, Spectra-Physics, Newport) with an 80 MHz repetition rate was used to provide pump and Stokes beams. The 120 fs pump laser at 934 nm was coupled into a 0.3 m polarization-maintaining single-mode fiber (PMSMF) and then delivered into a 4f pulse shaper system consisting of a grating (1800 l/mm@840 nm, Wasatch Photonics) and a slit on a motorized stage. The intensity of a 1040 nm Stokes laser was modulated by an acousto-optic modulator (AOM) at a frequency of 2.7 MHz. The Stokes laser was further sent to a spectral compressor, which is composed of a grating pair (1000 l/mm, LSFSG-1000, LightSmyth) with a distance of 15 cm and a 15 m PMSMF. The pump and Stokes laser were combined by a dichroic mirror (DMSP1000, Thorlabs) and delivered to a two-dimensional (2D) galvanometer for SRS imaging. In the detection end, the Stokes beam was blocked by two short-pass filters (ET980sp, Chroma). The SRS signal was detected by a homemade photodiode (PD) with a resonant amplifier and a lock-in amplifier (HF2 LI, Zurich Instruments). In addition, the pulse width of a pump laser after the pulse shape was measured to be ~2.5 ps by an autocorrelator (CARPE, APE). To measure the pulse width of the Stokes laser (~6.5 ps), we used a two-photon signal of rhodamine 6G by a time delay line. The sensitivity of our system is shown in Figure S1.

Sample Preparation. The saturated fatty acid samples used in the experiment are purchased from Macklin. Individual solid saturated fatty acids are crushed into powder and placed between glass slides. The mixed sample is crushed and placed in an EP tube to be shaken evenly and placed in an ultrasonic machine for further mixing.

Experimental Settings. In our experiments, the power of the Stokes laser was measured to be 300 mW before the galvanometer. The power of the pump laser was 400 mW before pulse shaping and degraded to 3 mW after pulse shaper with a slit size close to 75 μm. The spontaneous Raman spectra were obtained by a home-built 671 nm Raman spectroscope. A 60× objective (N.A. 1.2, UPLSAPO 60XW) and a 40× objective (N.A. 0.9, UPLSAPO) were used in obtaining SRS spectra and imaging, respectively. The dwell time was 80 μs in imaging. The imaging result was stitched by four spectral images to form a large field of view of about 900 μm.

RESULTS AND DISCUSSION

The schematic setup of our hyperspectral SRS imaging system is depicted in Figure 1. The fs 934 nm pump laser at about 1 W high power was intentionally broadened in spectrum to 12 nm (full width at half-maximum, FWHM) by the nonlinear effect called self-phase modulation (SPM) in a 0.3 m long polarization-maintaining single-mode fiber (PMSMF). A 4f pulse shaper consisting of holographic grating, achromatic lens, and slit played the key role of wavelength scanning for spectral imaging.[24] The ultimate spectral resolution of our pulse shaper can reach 2.5 cm^{-1} as the selective slit opened on the Fourier plane of the spanned spectrum is tuned to a minimum (Figure S2a).[25] Conversely, the spectral width of the Stokes laser was compressed by a spectral compressor, in which a grating pair with a separation of 15 cm provided negative chirping for spectral compression and a 15 m long PMSMF fulfilled the spectral compression.[26] It is worth noting that the nonlinear effect of SPM will induce spectral broadening as the input fs laser is positively chirped but result in spectral narrowing for the negatively chirped pulse. The spectral compressor is rather efficient. Including the laser power loss in the grating pair and

https://doi.org/10.1021/acs.analchem.3c00291
Anal. Chem. 2023, 95, 5815−5819

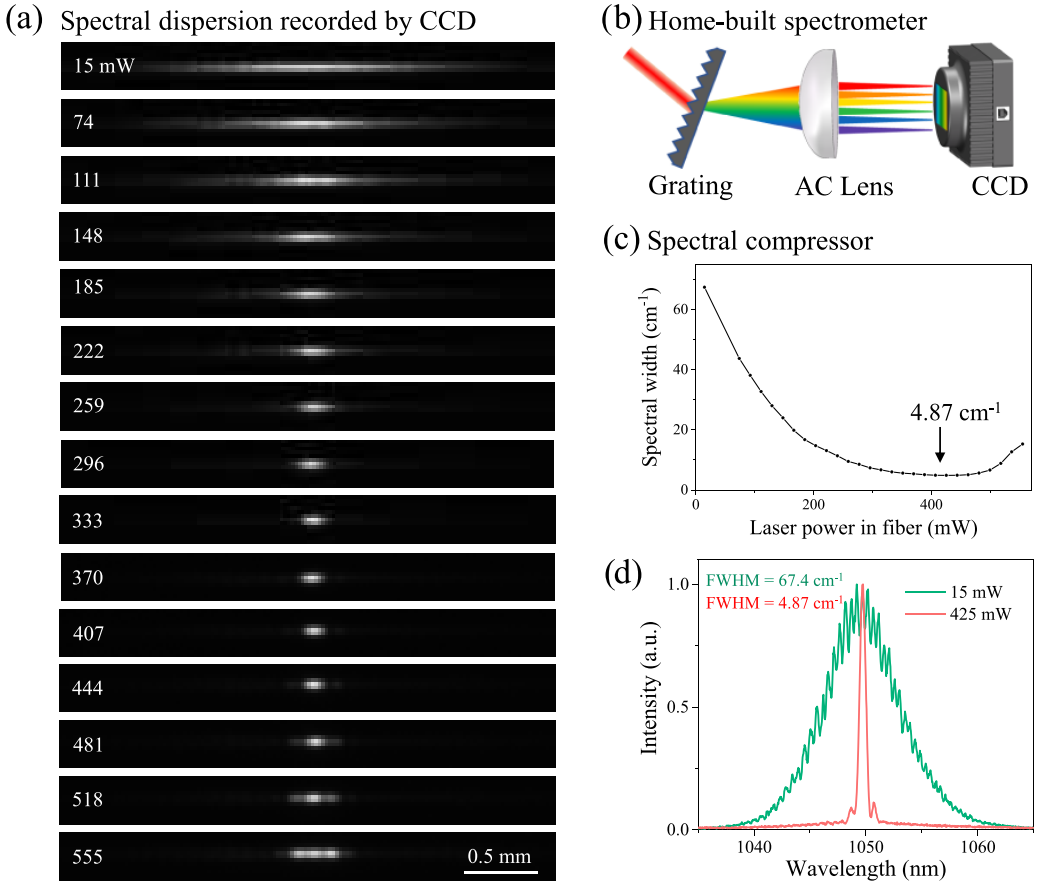

Figure 2. Spectral width measurement after the spectral compressor. (a) Spatially dispersed beam shape of the Stokes laser. The images were recorded by a home-built spectrometer shown in panel (b). As the laser power delivered into the fiber was less than 15 mW, the spectral width represents the original bandwidth of the fs Stokes laser. As the laser power was gradually increased to 555 mW, the spectral width was narrowed to a minimum at 425 mW and broadened again. (b) A home-built spectrometer. (c) Spectral width as a function of laser power in the fiber. (d) The spectral profile and width recorded at low laser power (15 mW) and high laser power (425 mW).

fiber coupling, the complete transmission efficiency of our spectral compressor is ∼65%.

To achieve the optimal spectral width, we gradually increase the Stokes laser power in fiber. As shown in Figure 2a, the spectra of the Stokes laser were spanned and recorded by a home-built spectrometer (Figure 2b). As the laser power was tuned up, the narrowing of spectral width was observed vividly. At a laser power of 425 mW, the spectral width reached a record of about 4.87 cm^{-1} in our experiment, which was the minimum and the turning point for the spectral compression process (Figures 2c and S2b). In contrast to the original spectral width of about 67 cm^{-1} (corresponding to ∼100 fs laser in pulse width), the compression ratio reached 13.8 (Figure 2d). For shorter fibers with less SPM effect, the compression ratio will be significantly reduced (Figure S3). Thus, by direct convolution of the line width of pump (2.5 cm^{-1}) and Stokes lasers (4.87 cm^{-1}), the spectral resolution of our SRS system can reach 5.4 cm^{-1} in theory. In fact, by utilizing longer fiber for the Stokes laser, a higher compression ratio and narrower bandwidth are straightforward. However, the pulse width will be broadened to >20 ps, which is no longer applicable for SRS imaging.

With such high spectral resolution, we performed hyperspectral SRS imaging of a series of saturated fatty acids, including caprylic acid (C8, C8:0), capric acid (C10, C10:0), lauric acid (L12, C12:0), myristic acid (M14, C14:0), palmitic acid (P16, C16:0), stearic acid (S18, C18:0), arachidic acid (A20, C20:0), and behenic acid (B22, C22:0). As shown in Figure 3a,b, we compared the Raman spectra and SRS spectra of these straight-chain fatty acids. With chain length increasing from 8 to 22 carbons, the Raman bands of alkyl C−C gauche stretches present a consecutively red-shifting with a step of about 5 cm^{-1} in a 40 cm^{-1} spectral range between 1070 and 1120 cm^{-1} (C10, 1074 cm^{-1}; L12, 1085; M14, 1093; P16, 1099; S18, 1103; A20, 1105; B22, 1111; see the magenta arrow in Figure 3b). Meanwhile, the Raman bands of alkyl C−C trans stretches at ∼1125 cm^{-1} exhibit comparatively less shifting but apparent correlation with chain lengths (see the blue arrow in Figure 3b). Thanks to the superior pulse shaper and spectral compressor employed in our system, the SRS spectra in Figure 3b clearly distinguished six Raman peaks between 1066 and 1088 cm^{-1}, corresponding to C12:0−C22:0, and proved a significantly better spectral resolution than the corresponding spontaneous Raman spectra in Figure 3a. The plotted curves in Figure 3c indicate that the Raman bands of the C−C gauche stretching almost linearly increased with the chain lengths with a step of about ∼5 cm^{-1}. However, the variation of the C−C trans stretching band features saturation with increased chain length (Figure 3d).

To validate the possibility of direct microscopic imaging of carbon chain lengths in complex conditions, we performed hyperspectral SRS mapping of a mixture phantom with six saturated fatty acids (C10:0−C20:0). SRS spectra were

https://doi.org/10.1021/acs.analchem.3c00291
Anal. Chem. 2023, 95, 5815−5819

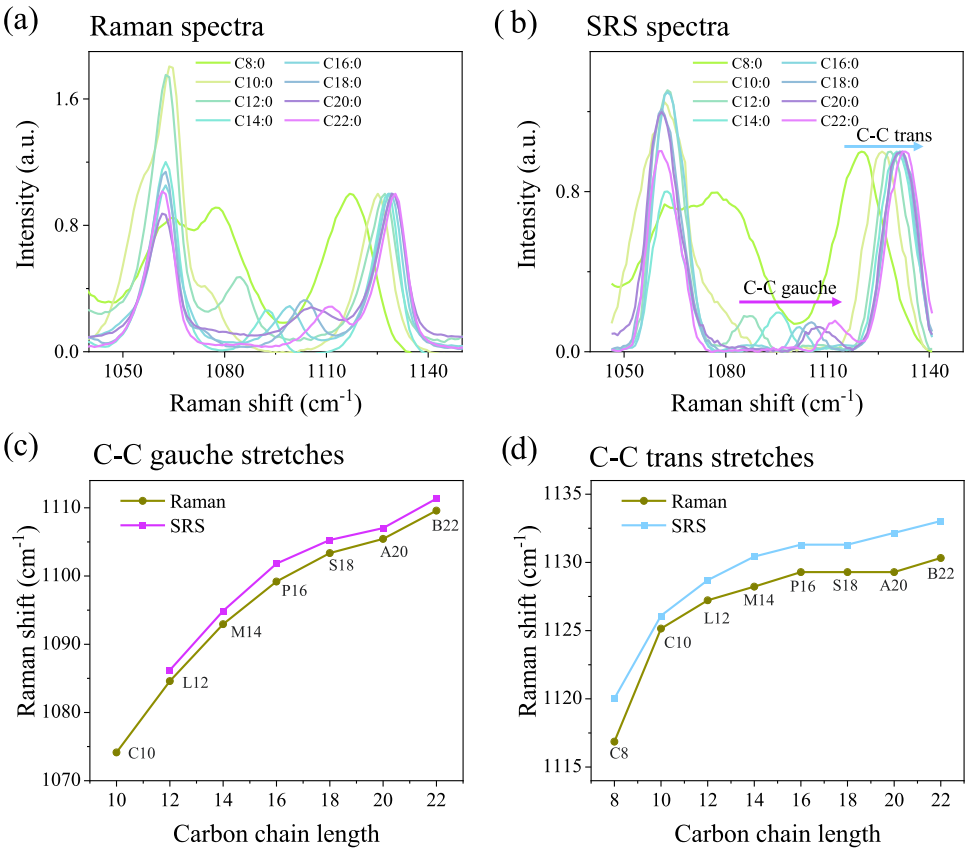

Figure 3. Raman and SRS spectra of various saturated fatty acids. (a) Spontaneous Raman spectra of lipids with chain lengths from C8:0 to C22:0. (b) The corresponding SRS spectra. The arrows indicate the directions of Raman shifts as the chain length increases. (c) Raman shifts of alkyl C−C gauche stretches depending on carbon chain lengths. (d) Raman shifts of alkyl C−C trans stretches depending on carbon chain lengths.

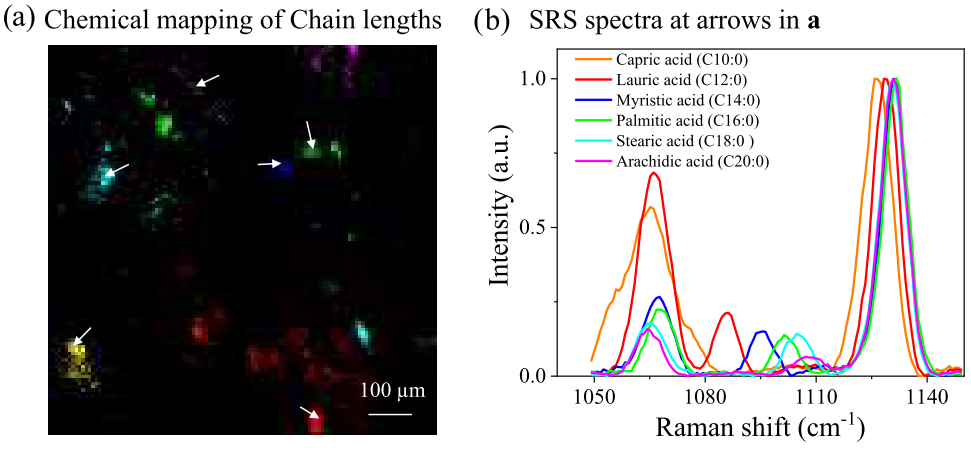

Figure 4. MCR retrieved concentration map and SRS spectra of C10:0−C20:0. (a) Concentration image of C8:0−C22:0. (b) SRS spectra obtained at the locations indicated by white arrows.

obtained in each image pixel for accurate chemical analysis. As shown in Figure 4a, different fatty acids were identified and quantitatively imaged by their Raman spectra, reflecting specific chain lengths. To illustrate their concentration distributions, we employed multivariate curve resolution (MCR) algorithm to reconstruct the spatial maps of different fatty acids and retrieve their corresponding Raman spectra in Figure 3b.

■ CONCLUSIONS

Fatty acids play essential roles in biological tissue metabolism. The in situ characterization of lipid chain lengths in diseased tissues will be of particular importance. In this work, we developed a hyperspectral SRS microscope with a superior spectral resolution of 5.4 cm^{-1} and allowed precious capability to resolve subtle Raman shifts corresponding to chain lengths. The proof-of-concept experiments were demonstrated to image chain lengths directly in a lipid phantom, consisting of mixed saturated fatty acids (C10:0−C20:0). The proposed chain length mapping method with further enhancement in sensitivity will for sure contribute to a variety of important biological and clinical applications in future.

https://doi.org/10.1021/acs.analchem.3c00291
Anal. Chem. 2023, 95, 5815−5819

■ ASSOCIATED CONTENT

Supporting Information

The Supporting Information is available free of charge at https://pubs.acs.org/doi/10.1021/acs.analchem.3c00291.

Evaluating the sensitivity and spectral resolution of the system (PDF)

■ AUTHOR INFORMATION

Corresponding Author

Shuai Yan − *Britton Chance Center and MoE Key Laboratory for Biomedical Photonics, Advanced Biomedical Imaging Facility, Wuhan National Laboratory for Optoelectronics-Huazhong University of Science and Technology, Wuhan 430074 Hubei, China; Changping Laboratory, Beijing 102206, China;* orcid.org/0000-0002-9083-7749; Email: Shuai_Yan@hust.edu.cn

Authors

Zhiliang Huang − *Britton Chance Center and MoE Key Laboratory for Biomedical Photonics, Advanced Biomedical Imaging Facility, Wuhan National Laboratory for Optoelectronics-Huazhong University of Science and Technology, Wuhan 430074 Hubei, China*

Yiran Li − *Britton Chance Center and MoE Key Laboratory for Biomedical Photonics, Advanced Biomedical Imaging Facility, Wuhan National Laboratory for Optoelectronics-Huazhong University of Science and Technology, Wuhan 430074 Hubei, China*

Wei Ju − *Britton Chance Center and MoE Key Laboratory for Biomedical Photonics, Advanced Biomedical Imaging Facility, Wuhan National Laboratory for Optoelectronics-Huazhong University of Science and Technology, Wuhan 430074 Hubei, China*

Ping Wang − *Britton Chance Center and MoE Key Laboratory for Biomedical Photonics, Advanced Biomedical Imaging Facility, Wuhan National Laboratory for Optoelectronics-Huazhong University of Science and Technology, Wuhan 430074 Hubei, China; Changping Laboratory, Beijing 102206, China; Research Center for Humanoid Sensing, Zhejiang Laboratory, Hangzhou 311100 Zhejiang, China; Optics Valley Laboratory, Wuhan 430074 Hubei, China; Huaiyin Institute of Technology, Huai'an 223001 Jiangsu, China;* orcid.org/0000-0002-5168-6829

Complete contact information is available at: https://pubs.acs.org/10.1021/acs.analchem.3c00291

Author Contributions

#Z.H. and S.Y. contributed equally. Z.H. and S.Y. carried out the construction of the stimulated Raman scattering microscope and performed all experiments. Z.H., S.Y., Y.L., W.J., and P.W. analyzed the data. S.Y., Z.H., W.J., and P.W. wrote the manuscript with inputs from all authors. S.Y. and P.W. conceived the concept and supervised the project.

Notes

The authors declare no competing financial interest.

■ ACKNOWLEDGMENTS

The authors thank the support from Analytical and Testing Center (HUST) and the Optical Bioimaging Core Facility of WNLO-HUST. S.Y. acknowledges the support from China Postdoctoral Science Foundation (2021M701322) and the funding for Postdoctoral Innovation Research Post in Hubei Province. P.W. acknowledges the support from the National Natural Science Foundation of China (62075076), the Innovation Project of Optics Valley Laboratory (OVL2021BG010), and the Innovation Fund of the Wuhan National Laboratory for Optoelectronics.

■ REFERENCES

(1) Yue, S.; Li, J.; Lee, S. Y.; Lee, H. J.; Shao, T.; Song, B.; Cheng, L.; Masterson, T. A.; Liu, X.; Ratliff, T. L.; Cheng, J. X. *Cell Metab.* **2014**, *19*, 393−406.

(2) Yan, S.; Cui, S. S.; Ke, K.; Zhao, B. X.; Liu, X. L.; Yue, S. H.; Wang, P. *Anal. Chem.* **2018**, *90*, 6362−6366.

(3) Li, J.; Condello, S.; Thomes-Pepin, J.; Ma, X.; Xia, Y.; Hurley, T. D.; Matei, D.; Cheng, J. X. *Cell Stem Cell* **2017**, *20*, 303−314.

(4) Paul, A.; Wang, Y.; Brännmark, C.; Kumar, S.; Bonn, M.; Parekh, S. H. *Biophys. J.* **2019**, *116*, 2346−2355.

(5) Suzuki, Y.; Kobayashi, K.; Wakisaka, Y.; Deng, D.; Tanaka, S.; Huang, C.-J.; Lei, C.; Sun, C.-W.; Liu, H.; Fujiwaki, Y.; Lee, S.; Isozaki, A.; Kasai, Y.; Hayakawa, T.; Sakuma, S.; Arai, F.; Koizumi, K.; Tezuka, H.; Inaba, M.; Hiraki, K.; Ito, T.; Hase, M.; Matsusaka, S.; Shiba, K.; Suga, K.; Nishikawa, M.; Jona, M.; Yatomi, Y.; Yalikun, Y.; Tanaka, Y.; Sugimura, T.; Nitta, N.; Goda, K.; Ozeki, Y. *Proc. Natl. Acad. Sci. U.S.A.* **2019**, *116*, 15842−15848.

(6) Kumamoto, Y.; Harada, Y.; Takamatsu, T.; Tanaka, H. *Acta Histochem. Cytochem.* **2018**, *51*, 101−110.

(7) Ji, M.; Orringer, D. A.; Freudiger, C. W.; Ramkissoon, S.; Liu, X.; Lau, D.; Golby, A. J.; Norton, I.; Hayashi, M.; Agar, N. Y.; Young, G. S.; Spino, C.; Santagata, S.; Camelo-Piragua, S.; Ligon, K. L.; Sagher, O.; Xie, X. S. *Sci. Transl. Med.* **2013**, *5*, No. 201ra119.

(8) Zhang, L.; Min, W. *J. Biomed. Opt.* **2017**, *22*, No. 106010.

(9) Iino, T.; Hashimoto, K.; Asai, T.; Kuchitsu, K.; Ozeki, Y. *Analyst* **2021**, *146*, 1234−1238.

(10) Min, W.; Freudiger, C. W.; Lu, S.; Xie, X. S. *Annu. Rev. Phys. Chem.* **2011**, *62*, 507−530.

(11) Fu, D.; Holtom, G.; Freudiger, C.; Zhang, X.; Xie, X. S. *J. Phys. Chem. B* **2013**, *117*, 4634−4640.

(12) Ji, M.; Lewis, S.; Camelo-Piragua, S.; Ramkissoon, S. H.; Snuderl, M.; Venneti, S.; Fisher-Hubbard, A.; Garrard, M.; Fu, D.; Wang, A. C.; Heth, J. A.; Maher, C. O.; Sanai, N.; Johnson, T. D.; Freudiger, C. W.; Sagher, O.; Xie, X. S.; Orringer, D. A. *Sci. Transl. Med.* **2015**, *7*, No. 309ra163.

(13) Freudiger, C. W.; Min, W.; Saar, B. G.; Lu, S.; Holtom, G. R.; He, C.; Tsai, J. C.; Kang, J. X.; Xie, X. S. *Science* **2008**, *322*, 1857−1861.

(14) Gong, L.; Zheng, W.; Ma, Y.; Huang, Z. *Nat. Photonics* **2020**, *14*, 115−122.

(15) Bae, K.; Zheng, W.; Huang, Z. *Theranostics* **2020**, *10*, 312−322.

(16) Ozeki, Y.; Umemura, W.; Otsuka, Y.; Satoh, S.; Hashimoto, H.; Sumimura, K.; Nishizawa, N.; Fukui, K.; Itoh, K. *Nat. Photonics* **2012**, *6*, 845−851.

(17) Lu, F. K.; Calligaris, D.; Olubiyi, O. I.; Norton, I.; Yang, W.; Santagata, S.; Xie, X. S.; Golby, A. J.; Agar, N. Y. *Cancer Res.* **2016**, *76*, 3451−3462.

(18) Wang, P.; Li, J.; Wang, P.; Hu, C. R.; Zhang, D.; Sturek, M.; Cheng, J. X. *Angew. Chem.* **2013**, *125*, 13280−13284.

(19) Jamieson, L. E.; Li, A.; Faulds, K.; Graham, D. *R. Soc. Open Sci.* **2018**, *5*, No. 181483.

(20) Allen, A. C.; Romero-Mangado, J.; Adams, S.; Flynn, M.; Chen, B.; Zhang, J. Z. *J. Phys. Chem. B* **2018**, *122*, 8396−8403.

(21) Wu, H.; Volponi, J. V.; Oliver, A. E.; Parikh, A. N.; Simmons, B. A.; Singh, S. *Proc. Natl. Acad. Sci. U.S.A.* **2011**, *108*, 3809−3814.

(22) Saggu, M.; Liu, J.; Patel, A. *Pharm. Res.* **2015**, *32*, 2877−2888.

(23) Chan, J. W.; Motton, D.; Rutledge, J. C.; Keim, N. L.; Huser, T. *Anal. Chem.* **2005**, *77*, 5870−5876.

(24) Zhang, D.; Wang, P.; Slipchenko, M. N.; Ben-Amotz, D.; Weiner, A. M.; Cheng, J. X. *Anal. Chem.* **2013**, *85*, 98−106.

(25) Weiner, A. M. *Opt. Commun.* **2011**, *284*, 3669−3692.

(26) Washburn, B. R.; Buck, J. A.; Ralph, S. E. *Opt. Lett.* **2000**, *25*, 445−447.